

Technological characterization of ceramic material originated from São José do Rio Pardo

Marcus Vinícius Fávero Alves¹ 
Maria Eduarda Simões Machado Oliveira¹ 
Guilherme Rodrigues de Paula da Silva¹ 
Carolina Del Roveri¹ 
Thamara Machado de Oliveira Ruellas² 
Sylma Carvalho Maestrelli^{1*} 

Abstract

This paper reports the characterization of a ceramic material originated from the hydrographic basin of the Fartura River, located in the city of São José do Rio Pardo, state of São Paulo, Brazil and, based on the results, proposes a destination for this material in the industry. The characterization was carried out using the techniques: X-Ray Diffraction (XRD), X-Ray Fluorescence (XRF), Specific Surface Area (B.E.T.), Thermal Analysis (TG/DSC), Real Density by Pycnometry, Cation Exchange Capacity (CEC), Maximum Solids Concentration, Plasticity Index (PI), Green Density (GD), Apparent Density (AD), Apparent Porosity (AP) and Linear Shrinkage (LS). The results indicated that the material is mainly composed of kaolinite, muscovite mica and quartz, in addition to goethite, siderite and titanite. The presence of a higher iron and titania content favored obtaining red-toned bodies after ceramic firing. Based on these results, the high plasticity and other tests performed, the investigated material was identified as a clay material, with good potential for industrial use in the production of lower-cost red ceramics, such as tiles, bricks, and red-fired coatings.

Keywords: Ceramics; Fartura River; São José do Rio Pardo; Technological characterization; Clays.

1 Introduction

Clays are a class of materials that have a large number of applications due to their physical-chemical characteristics, such as plasticity, easy conformation, and high mechanical resistance after firing, factors that have made their use timeless, going back about 25,000 years to primitive peoples in Europe and Asia [1-10].

Technically clays can be defined as natural earthy materials, fine-grained, with diameters of less than 2 μm , and that acquire a certain plasticity when wet [11,12]. Their constitution is essentially given by small particles of materials called argillominerals, and their formation results from weathering or hydrothermal action [5-13]. This leads to a wide variety of compositions and, consequently, to a wide range of applications [11]. Thus, the knowledge of the characteristics and physicochemical, mechanical, and rheological properties, as well as the knowledge of the argillominerals present is fundamental for the understanding of which ceramic sectors can benefit from this raw material [14].

In Brazil, several regions have soils rich in good-quality clay materials. In the interior of the state of São Paulo, more specifically in the municipality of São José do

Rio Pardo, in the hydrographic basin of the Fartura River, the presence of clay material with potential industrial use was identified [15].

This paper investigated the potential application of clay material from the region of the Fartura River basin based on its technological characterization, from tests of thermal, physical-chemical, and rheological characterization. Figure 1 [15] indicates the region from where the characterized clay material was extracted.

2 Experimental

The clay material collected near the Fartura River, in the municipality of São José do Rio Pardo, state of São Paulo, Brazil (location indicated in Figure 2 and Figure 3), was dried at 110 °C and deagglomerated on an 80-mesh sieve, resulting in a thin powder of a light gray color. Assays for X-Ray Diffraction (XRD), X-Ray Fluorescence (XRF), Specific Surface Area (B.E.T.), Thermal Analysis (TG/DSC), Real Density by Pycnometry, Cation Exchange

¹Instituto de Ciência e Tecnologia, Universidade Federal de Alfenas, UNIFAL-MG, Poços de Caldas, MG, Brasil.

²Dipartimento di Chimica, Università di Roma La Sapienza, Rome, RM, Italia.

*Corresponding author: sylma.maestrelli@unifal-mg.edu.br



Capacity (CEC), Plasticity Index (PI) and rheological characterization (maximum solids concentration) were performed on the powder.

The X-Ray Diffraction (XRD) test was performed using a copper tube ($K\alpha = 0.1542$ nm), with an accelerating potential of 40 kV and a current of 30 mA, in continuous

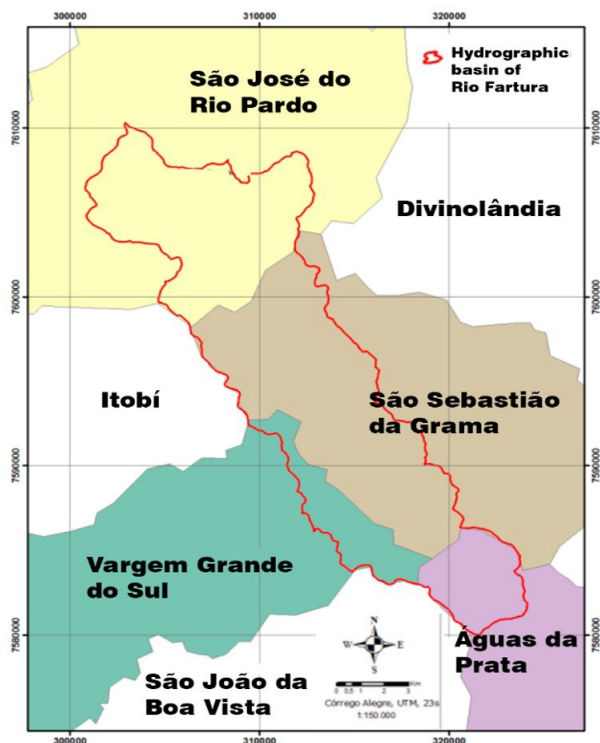


Figure 1. Demarcation of the hydrographic basin of the Fartura River, in which the yellow color indicates the municipality of São José do Rio Pardo.

angular scanning from 5° to 70° at a rate of 0.05° per minute. The peaks were identified and indexed using the JCPDS-ICDD (Joint Committee on Powder Diffraction Standards - International Centre for Diffraction Data) Powder Diffraction File (PDF) 2003 database. Chemical analysis via X-ray fluorescence (XRF) was conducted using the Axios PW 4400/40 DY 1686 equipment. For XRF analysis, the beads were prepared using a lithium tetraborate ($\text{Li}_2\text{B}_4\text{O}_7$) fluxing agent at 99.5% and 0.5% lithium bromate (LiBr) in a platinum-gold crucible.

The specific surface area was measured using the nitrogen physisorption method based on the B.E.T. technique, employing a Micromeritics ASAP 2020 instrument at a temperature of 77 K. The TG/DSC analyses were concomitantly performed on a Netzsch Jupiter STA 449 F3 instrument. Approximately 10 mg of the material was analyzed in a platinum-rhodium alloy crucible, under a Nitrogen atmosphere, with a heating rate of $10^\circ\text{C}/\text{min}$.

The determination of Cation Exchange Capacity (CEC) was carried out in triplicate, following the Standard Test Method for Methylene Blue Index of Clay, as per ASTM C837-81 [16]. This method utilizes the linear correlation between the methylene blue index and key clay properties, such as CEC and specific surface area. The Plasticity Index (PI) test was conducted in accordance with ASTM D423-66 [17] for the Liquid Limit (LL) and ASTM D424-59 [18] for the Plastic Limit (PL).

The maximum solids concentration was determined using sodium silicate (provided by Vetec Química Fina) as a deflocculant. This sodium silicate contains 25% sodium oxide and 30% silicon oxide, with a pH between 11 and 13, and 42% water content. The test was conducted using a Fungilab ADV R viscometer, set to operate at 100 rpm, with an R5 spindle.



Figure 2. Region from where the material was extracted. Point A indicates the sample collection site and point B is the affluent (aerial image).



Figure 3. Site excavated for sample collection.

In the maximum solids concentration test, the experimentally determined density of the sodium silicate deflocculant was 1.79 g/cm^3 . The density of the suspension was calculated to be 1.36 g/cm^3 , taking into account the actual densities of the ceramic powder and the water. For this test, the suspension was prepared using 272 g of solid content.

After the addition of 10% water by weight and homogenization on an 80-mesh sieve, the powder was shaped by uniaxial pressing, in the form of rectangular bars of $70 \times 20 \times 7 \text{ mm}$, applying a pressure of 275 MPa, and its green density was then determined, by geometrical method, after drying in an oven at $60 \text{ }^\circ\text{C}$ for 24 h. The ceramic firing of the bars was carried out with a heating rate of $5 \text{ }^\circ\text{C/min}$ and a plateau of 2h, varying the temperatures ($850 \text{ }^\circ\text{C}$, $950 \text{ }^\circ\text{C}$, $1000 \text{ }^\circ\text{C}$ and $1150 \text{ }^\circ\text{C}$). Measurements of Apparent Density (AD) and Apparent Porosity (AP) for each firing condition were obtained using the Archimedes method, following the ASTM C373-88 standard [19]. Linear Shrinkage (LS) was determined in accordance with ASTM C326-09 [20].

3 Results and discussion

The XRD results (Figure 4) indicated that the material under study is a clay mineral constituted mostly by materials commonly found in the region from where it was extracted, namely: kaolinite (hydrated aluminum silicate), muscovite mica (phyllosilicate) and quartz, besides goethite and siderite (in which the presence of iron is high) and titanite (titanium and calcium silicate).

The XRF results (Table 1) corroborate those obtained by XRD. Table 1 shows that the chemical composition of the sample is mostly of, respectively, medium percentages of silica (SiO_2) and alumina (Al_2O_3), with silica found in the crystalline phase quartz and in aluminosilicates, when combined with alumina. The amount of free silica is inversely proportional to plasticity and shrinkage. Alumina, on the other hand, is generally found as a constituent of the structure of aluminosilicates, such as kaolinite [21], a fact corroborated by the XRD results. The presence of iron oxide (Fe_2O_3) in a percentage over 4% is responsible for giving the bar a red

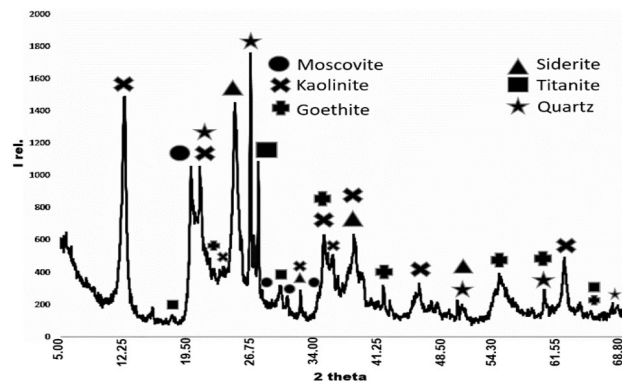


Figure 4. Diffractogram of the investigated ceramic material.

Table 1. Chemical composition of the investigated material

Oxide or Event	Mass content (%)
Loss on ignition	10.92
Al_2O_3	29.24
SiO_2	49.64
TiO_2	1.37
Fe_2O_3	4.37
CaO	0.36
MgO	0.90
Na_2O	0.26
K_2O	1.95
CrO_3	0.13
P_2O_5	0.33

tone after firing. In addition, the presence of titanium oxide (TiO_2) also contributes to the post-firing color towards an orange tone, and thus, together with iron oxide, they are the main chromophore agents [22-24]. The main sources of iron (goethite and siderite) and titanium (titanite) were further found in the XRD. Goethite is an antiferromagnetic material and siderite has a weak (paramagnetic) magnetism [25]. Thus, the reduction of the iron content in the material in order to ease the red tone of the bodies after firing (for applications in light-fired ceramics) is difficult due to the non-magnetic characteristics. In addition, there is evidence of sodium (Na_2O) and potassium (K_2O) oxides, alkali oxides, originated from the muscovite, that act as melting agents [26], contributing to the formation of the liquid phase and subsequent sintering. The presence of magnesium (MgO) and calcium (CaO) oxides is also associated with melting agents. These oxides can interact with amorphous phases, forming crystalline phases that are more stable towards the action of humidity [21]. The loss on ignition, on the other hand, indicates that the ceramic material has a considerable presence of organic material, which is eliminated after firing.

The specific surface area by B.E.T. value obtained was $43.547 \text{ m}^2/\text{g}$. In comparison, kaolinitic clays from Warren

County, Georgia and San Bernardino County, California [27] had values of 13.1 m²/g and 21.7 m²/g, respectively, being their specific surface areas considerably lower than that of the material investigated in this paper. When analyzing kaolinite samples [28], values between 18.7 m²/g and 25.9 m²/g were obtained, which were also lower. The larger specific surface area of the investigated sample is a very positive result, since it favors greater reactivity of the powder during firing, contributing to less porosity and more dense and mechanically resistant bodies [29].

It is also worth noting that the presence of melting agents, as already reported in Table 1, also favors the reduction of porosity due to the sintering mechanism via the liquid phase. This method is cost-effective due to its lower temperature requirement for porosity reduction compared to solid-phase sintering. From an industrial perspective, it also offers faster processing.

Figure 5 shows the results obtained from the TG/DSC analysis. The loss in the region between 150 °C and 300 °C is related to the elimination of organic matter [30], and it is comparable to the values obtained by XRF, which indicates a loss on ignition of 10.92%, further evidencing the presence of organic matter in the sample. The loss of physically adsorbed water is also observed [30,31]. The differential scanning calorimetry curve distinguishes a significant endothermic event (inverted peak) in the region between 400 °C and 500 °C, with the decreasing profile of the TG curve. This pronounced loss is attributed to the dihydroxylation of the argillominerals [32,33]. The other regions have small fluctuations due to the equipment itself.

The average real density was 2.51 ± 0.04 g/cm³, a value typically found for clay materials. Kaolins have densities around 2.65 g/cm³ [34], which is close to the value found experimentally.

The CEC assay (Figure 6) of the investigated material was 83.6 meq/100g. These values are similar when compared to studies of CEC in smectite clays, whose typical values are in the range of 100-150 meq/100g [35] and high when compared to kaolinites, with values between 2.8 and 10 meq/100g [36].

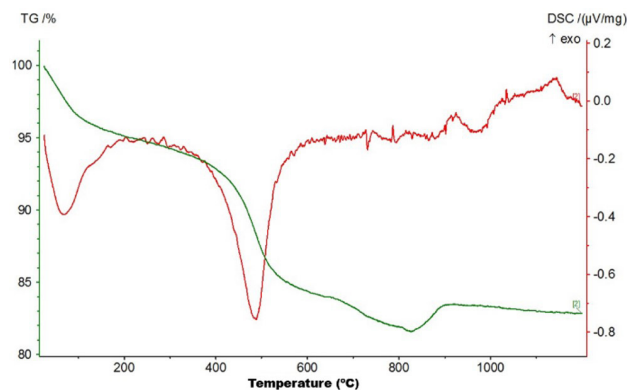


Figure 5. TG/DSC of the investigated sample.

Figure 7 shows the deflocculation graph of the material under study. The lowest suspension viscosity levels (80 mPa.s) are obtained when adding approximately 0.12% sodium silicate (or approximately 8 drops of deflocculant).

From the density values, the initial mass of ceramic powder (119.68 g) contained in the water volume (152.32 mL) was calculated, and with subsequent additions of 20 g of powder, the graph in Figure 8 was constructed.

Figure 8 indicates that the maximum percentage of solids is 66% by weight in relation to the suspension mass.

The values obtained for the liquid and plastic limits were 64.11 and 29.94, respectively, resulting in a plasticity index (PI) equal to 34.97, which classifies the investigated material as highly plastic. The result is quite positive since materials with high plasticity are more easily conformable and tend to present fewer problems during the drying and firing stages, provided they are performed under the right conditions. This expands the range of forming techniques for the investigated material and, consequently, the different possibilities of products to launch on the market.

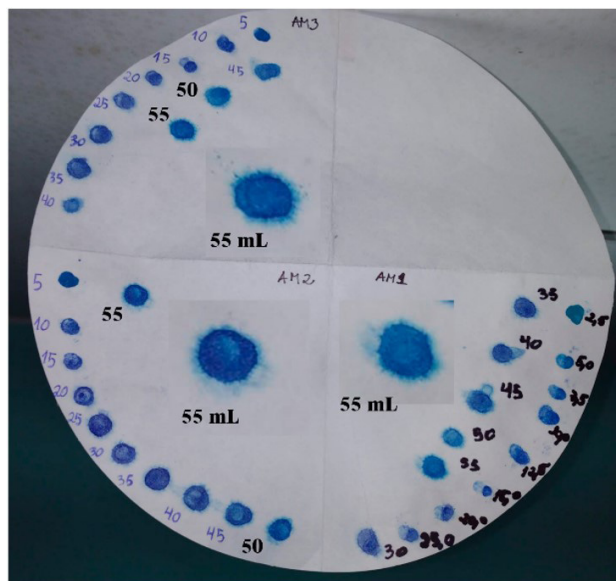


Figure 6. CEC assay for the investigated material.

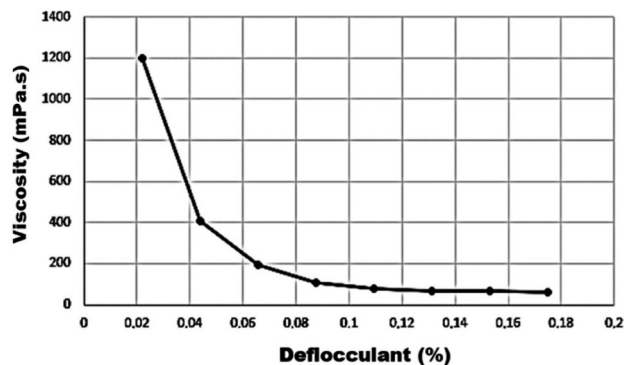


Figure 7. Graph of deflocculant mass percentage by viscosity.

The average green density value was $1.93 \pm 0.05 \text{ g/cm}^3$. Given the actual density value of 2.51 g/cm^3 , the samples presented high green density, which was attributed to the good fluidity of the powder and high plasticity, thus facilitating the compaction and the increase in green density. Figure 9 shows the powders compacted by uniaxial pressing into a bar shape before ceramic firing.

Figures 10 and 11 show the effect of firing temperature on the density and apparent porosity values, respectively. Figure 12 shows the influence of temperature on the linear shrinkage values of the samples.

Figures 10 and 11 show that the higher the firing temperature (in general), the higher the apparent density and the lower the porosity. Additionally, the samples were found to be quite reproducible, given the small deviations obtained both before and after firing.

The samples fired at 850°C and 950°C were statistically similar, which is associated with the low temperature of ceramic firing, insufficient to optimize all the sintering stages of the samples; that is, the time and temperature were not enough to promote greater pore closure and greater shrinkage. This is proven by the apparent porosity results, which are still reasonably high for the samples fired at lower temperatures. Above 1000°C an effective reduction in porosity takes place, with a consequent decrease in water

absorption and an increase in the linear shrinkage of the samples (Figure 12).

The decrease in porosity due to the increase in firing temperature is consistent with the data presented for water absorption, which decreases as the temperature increases because the samples are less porous.

Figure 13 shows an image of the samples to demonstrate the color tones obtained at the different firing temperatures

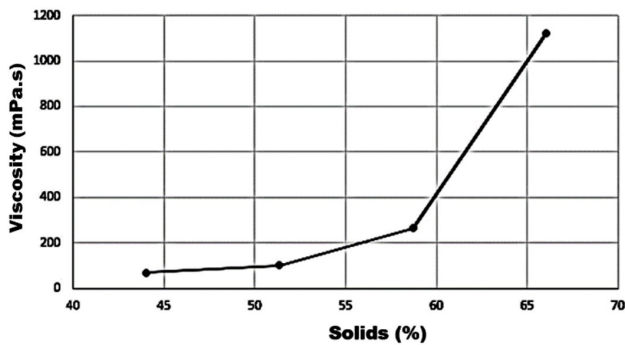


Figure 8. Graph of solids percentage by viscosity.

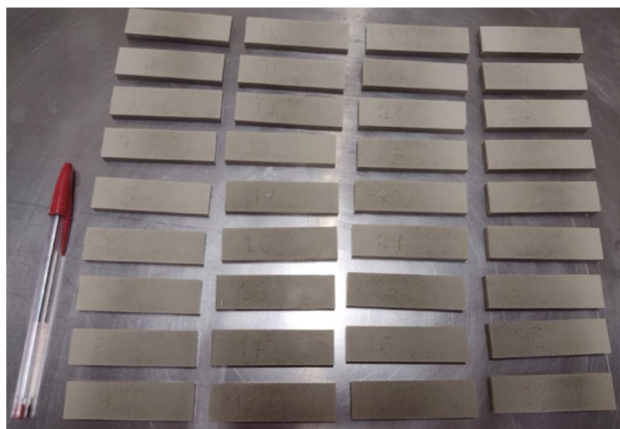


Figure 9. Ceramic powder conformed into bars by uniaxial pressing.

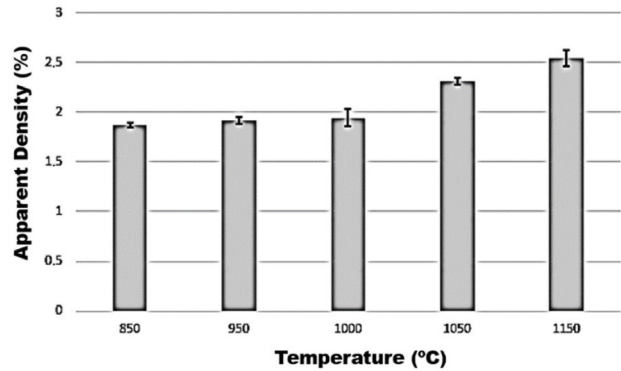


Figure 10. Graph of apparent density (g/cm^3) as a function of firing temperature.

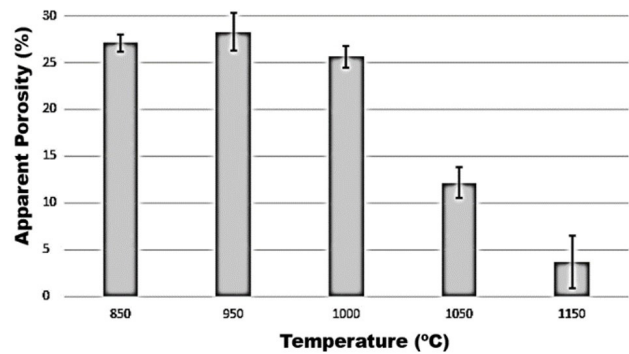


Figure 11. Graph of apparent porosity (%) as a function of firing temperature.

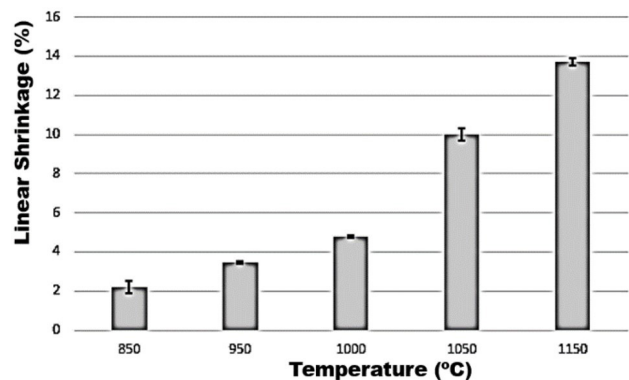


Figure 12. Graph of linear shrinkage (%) as a function of firing temperature.



Figure 13. Color of the samples after ceramic firing at temperatures of 850 °C, 950 °C, 1000 °C, 1050 °C and 1150 °C.

of 850°, 950°, 1000°, 1050°, and 1150 °C. After firing, the red color became noticeably more pronounced with increasing temperature, possibly due to the release of titanium present in titanite and iron from goethite and siderite, which puts forward the use of the material in the red ceramic sector.

4 Conclusions

The high specific surface areas and plasticity, in addition to the solid content and deflocculation curves, indicate that the material does not present problems associated with processing; that is, there is a wide range of applications, and the material may be shaped by both dry and wet techniques (pressing, extrusion, slip casting, replica, among others). Another prominent factor is the firing temperature and final porosity: the material investigated is suitable for firing at lower temperatures because sintering occurs via the liquid phase, which decreases production costs.

Thus, the material may be used in lower-cost red ceramic products, such as solid bricks, ceramic blocks (sealing and structural), roof tiles, pipes, lining slabs, and ornamental vases, among others.

Additionally, a more detailed study of the formulation and processing may bring new applications such as in monoporous coatings, which would add more value to the investigated material. An indication that supports this possible application lies in the fact that at 850 °C, 950 °C, and 1000 °C the water absorption was higher than 10% in addition to the occurrence of iron oxide in the material between 4% and 8%, two of the characteristics indicated for porous coatings. In this sense, further studies for this specific evaluation are required.

Acknowledgements

The authors would like to express their gratitude to the Crystallography Laboratory of the Federal University of Alfenas (Alfenas/MG campus) and for the availability to perform the assays at the Poços de Caldas/MG campus. They also gratefully acknowledge the company Togni Materiais Refratários S/A, Poços de Caldas/MG for supplying equipment. This study was also supported by the Coordenação de Aperfeiçoamento de Pessoal de Nível Superior – Brazil (CAPES) – Finance Code 001.

References

1. Odoma AN, Obaje NG, Omada JI, Idakwo SO, Erbacher J. Paleoclimate reconstruction during Mamu Formation (Cretaceous) based on clay mineral distributions. *IOSR Journal of Applied Geology and Geophysics*. 2013;1(5):40-46.
2. Angelo V. Preparation and catalytic properties of cationic and anionic clays. *Catalysis Today*. 1998;41(1-3):53-71. [http://dx.doi.org/10.1016/S0920-5861\(98\)00038-8](http://dx.doi.org/10.1016/S0920-5861(98)00038-8).
3. Aghris S, Laghrib F, Koumya Y, El Kasmi S, Azaitraoui M, Farahi A, et al. Exploration of a new source of sustainable aluminosilicate clay minerals from marocco: mineralogical and phisico-chemical characterization for clear upcoming application. *Journal of Inorganic and Organometallic Polymers*. 2021;31:2925-2938. <http://dx.doi.org/10.1007/s10904-021-01950-1>.
4. Wang G, Ran L, Xu J, Wang Y, Ma L, Zhu R, et al. Technical development of characterization methods provides insights into clay mineral-water interactions: a comprehensive review. *Applied Clay Science*. 2021;206:106088. <http://dx.doi.org/10.1016/j.clay.2021.106088>.
5. Mc Connell RL, Abel DC. *Environmental geology today*. Burlington: Jones & Bartlett Publishers; 2013.
6. Sari MY, Kalpakli Y, Piskin S. Thermal behavior and dehydroxylation kinetics of naturally occurring sepiolite and bentonite. *Journal of Thermal Analysis and Calorimetry*. 2013;114(3):1191-1199. <http://dx.doi.org/10.1007/s10973-013-3152-x>.

- 7 Janík R, Jóna E, Pavlík V, Lizák P, Mojumdar SC. Interactions of 2,5- and 3,5-dimethylphenols with co-exchanged montmorillonite. *Journal of Thermal Analysis and Calorimetry*. 2013;112(2):1083-1087. <http://dx.doi.org/10.1007/s10973-013-3012-8>.
- 8 Moraes JDD, Bertolino SRA, Cuffni SL, Ducart DF, Bretzke PE, Leonardi GR. Clay minerals: Properties and applications to dermocosmetic products and perspectives of natural raw materials for therapeutic purpose - a review. *International Journal of Pharmaceutics*. 2017;534(1-2):213-219. <http://dx.doi.org/10.1016/j.ijpharm.2017.10.031>.
- 9 Kooli F, Yan L, Tan SX, Zheng J. Organoclays from alkaline-treated acid-activated clays. *Journal of Thermal Analysis and Calorimetry*. 2013;115(2):1465-1475. <http://dx.doi.org/10.1007/s10973-013-3454-z>.
- 10 Arianpour AÇ, Arianpour F. Characterization, technological Properties, and ceramic applications of Kastamonu alluvial clay (Northern Turkey) in Building materials. *Construction & Building Materials*. 2022;356:129304. <http://dx.doi.org/10.1016/j.conbuildmat.2022.129304>.
- 11 Santos PS. *Ciência e tecnologia de argilas*. São Paulo: Editora Edgard Blucher Ltda; 1989.
- 12 Guggenheim S, Martin RT. Definition of clay and clay mineral: joint report of the AIPEA nomenclature and CMS Nomenclature Committees. *Clay Minerals*. 1995;30(3):257-259. <http://dx.doi.org/10.1180/claymin.1995.030.3.09>.
- 13 Muhammed NS, Olayiwola T, Elkhatatny S. A review on clay chemistry, characterization and shale inhibitors for water-based drilling fluids. *Journal of Petroleum Science Engineering*. 2021;206:109043. <http://dx.doi.org/10.1016/j.petrol.2021.109043>.
- 14 Santos RS. Interação entre características de argilas e parâmetros de processamento sobre propriedades tecnológicas de corpos cerâmicos. *Cerâmica*. 2017;63:361-368. <http://dx.doi.org/10.1590/0366-69132017633672126>.
- 15 Faleiros CA. Zoneamento geoambiental da bacia do Rio Fartura: abrangendo os municípios de São José do Rio Pardo - SP, São Sebastião da Gramma-SP, Vargem Grande do Sul-SP e Águas da Prata - SP, na escala 1:50.000 [tese]. São Carlos: Programa de Pós-graduação em Engenharia Urbana, Centro de Ciências Exatas e Tecnologia, Universidade Federal de São Carlos; 2012.
- 16 ASTM International. ASTM C837-81. West Conshohocken: ASTM International. Standard Test Method for Methylene Blue Index
- 17 ASTM International. ASTM D423-66. West Conshohocken: ASTM International. Standard Method of Test for Liquid Limit of Soils
- 18 ASTM International. ASTM D424-59. West Conshohocken: ASTM International. Standard Test Method for Plastic Limit and Plasticity
- 19 ASTM International. ASTM C373-88. West Conshohocken: ASTM International. Standard Test Method for Water Absorption, Bulk
- 20 ASTM International. ASTM C326-09. West Conshohocken: ASTM International. Standard Test Method for Drying and Firing Shrinkages
- 21 Gadioli MCB, Borlini JCG, Caranassios A. Characterization of clay from Vale do Mulemba-ES. *Materials Science Forum*. 2008;591:487-492. <http://dx.doi.org/10.4028/www.scientific.net/MSF.591-593.487>.
- 22 Agrawal P, Misra SN, Sharma T. Beneficiation of Low Grade Kaolin by High Shear Agitation with Dispersant (HSD) pre-treatment for high yield and improved fired colour. *Indian Ceramic Society*. 2014;73(1):48-57. <http://dx.doi.org/10.1080/0371750X.2014.890462>.
- 23 Llop J, Notari MD, Barrachina E, Nebot I, Nunez I, Carda JB. Clay treatment to improve its color parameters to use them in porcelain stoneware production. *La Sociedad Espanola de Ceramica y Vidrio*. 2010;49:413-422.
- 24 Motta JFM, Luz AB, Baltar CAM, Bezerra MS, Cabral M Jr, Coelho JM. RMIs: argila plástica para cerâmica branca. In: CETEM/MCTI. *Rochas e minerais industriais no Brasil: usos e especificações*. 2.ed. Rio de Janeiro: CETEM/MCTI; 2008. p. 771-791.
- 25 Valezi DF, Carneiro CEA, Costa ACS, Paesano A Jr, Spadotto JC, Solórzano IG, et al. Weak ferromagnetic component in goethite (α -FeOOH) and its relation with microstructural characteristics. *Materials Chemistry and Physics*. 2020;246:122851. <http://dx.doi.org/10.1016/j.matchemphys.2020.122851>.
- 26 Vieira CMF, Soares TM, Sánchez R, Monteiro SN. Incorporation of granite waste in red ceramics. *Materials Science and Engineering A*. 2004;373:115-121. <http://dx.doi.org/10.1016/j.msea.2003.12.038>.
- 27 Dogan M, Dogan AU, Yesilyurt FL, Alaygut D, Buckner DI, Wurster DE. Baseline studies of the Clay Minerals Society special clays: specific surface area by the Brunauer Emmett Teller (BET) method. *Clays and Clay Minerals*. 2007;55(5):534-541. <http://dx.doi.org/10.1346/CCMN.2006.0540108>.

- 28 Mbey JA, Thomas F, Razafitianamaharavo A, Caillet C, Villiéras F. A comparative study of some kaolinites surface properties. *Applied Clay Science*. 2019;172:135-145. <http://dx.doi.org/10.1016/j.clay.2019.03.005>.
- 29 Meloni P, Carcangiu G, Delogu F. Specific surface area and chemical reactivity of quartz powders during mechanical processing. *Materials Research Bulletin*. 2012;47(1):146-151. <http://dx.doi.org/10.1016/j.materresbull.2011.09.014>.
- 30 Macedo RS, Menezes RR, Neves GA, Ferreira HC. Estudo de argilas usadas em cerâmica vermelha. *Cerâmica*. 2008;54:411-417. <http://dx.doi.org/10.1590/S0366-69132008000400005>.
- 31 Maia LJQ, Martins TA, Gesicki ALD, Salvetti AR. Caracterização Térmica de argilas da cidade de Costa Rica no Estado de Mato Grosso do Sul. In: *Anais do 44º Congresso Brasileiro de Cerâmica; 2000; São Paulo, Brazil*. São Paulo: ABCERAM. p. 06101-06110.
- 32 Oba RNM, Ifo GM, Madila EEN, Diamouangana FZM, Vila T, Foutou MP, et al. Characterization of the clay collected in the locality of dolisie in Congo-Brazzaville. *Journal of Minerals and Materials Characterization and Engineering*. 2022;10(2):93-105. <http://dx.doi.org/10.4236/jmmce.2022.102007>.
- 33 Menezes RR, Souto PM, Santana LML, Neves GA, Kiminami RHGA, Ferreira HC. Argilas bentoníticas de Cubati, Paraíba, Brasil: caracterização física-mineralógica. *Cerâmica*. 2009;55:163-169. <http://dx.doi.org/10.1590/S0366-69132009000200008>.
- 34 National Center for Biotechnology Information. [National Library of Medicine]. Bethesda: National Center for Biotechnology Information; 2012 March 21, [2022 March 12]. <https://pubchem.ncbi.nlm.nih.gov/compound/Kaolin>
- 35 Deng Y, Liu L, Velázquez ALB, Dixon JB. The determinative role of the exchange cation and layer-charge density of smectite on aflatoxin ADSORTION. *Clays and Clay Minerals*. 2012;60(4):374-386. <http://dx.doi.org/10.1346/CCMN.2012.0600404>.
- 36 Ma C, Eggleton RA. Cation exchange capacity of kaolinite. *Clays and Clay Minerals*. 1999;47(2):174-180.

Received: 25 Sep. 2023

Accepted: 28 Nov. 2023